EPJ manuscript No.
(will be inserted by the editor)

Focusing and splitting of particle streams in microflows via viscosity gradients

Matthias Laumann and Walter Zimmermann

Theoretische Physik I, Universität Bayreuth, 95440 Bayreuth, Germany; E-mail: walter.zimmermann@uni-bayreuth.de

Received: date / Revised version: date

Abstract Microflows are intensively used for investigating and controlling the dynamics of particles, including soft particles such as biological cells and capsules. A classic result is the tank-treading motion of elliptically deformed soft particles in linear shear flows, which do not migrate across straight stream lines in the bulk. However, soft particles migrate across straight streamlines in Poiseuille flows. In this work we describe a new mechanism of cross-streamline migration of soft particles. If the viscosity varies perpendicular to the stream lines then particles migrate across stream lines towards regions of a lower viscosity, even in linear shear flows. An interplay with the repulsive particle-boundary interaction causes then focusing of particles in linear shear flows with the attractor stream line closer to the wall in the low viscosity region. Viscosity variations perpendicular to the stream lines in Poiseuille flows leads either to a shift of the particle attractor or even to a splitting of particle attractors, which may give rise to interesting applications for particle separation. The location of attracting streamlines depend on the particle properties, like their size and elasticity. The cross-stream migration induced by viscosity variations is explained by analytical considerations, Stokesian dynamics simulations with a generalized Oseen tensor and Lattice-Boltzmann simulations.

1 Introduction

The success of the interdisciplinary field of microfluidics and its numerous applications in life science and applications are based also on a thorough understanding of the dynamics of particles and their distribution in microflows. [1,2,3,4,5,6] One of the important applications is particle sorting where besides structured channels also optical, electrical or magnetic fields are used.[3] Several sorting strategies rely merely on the interplay between basic hydrodynamics of microflows and particle properties, that cause, for instance, cross-streamline migration (CSM) of particles. CSM may depend on fluid inertia,[5] on particle deformability, [7,8,9,10,11,12,13,14,15,16,17] on channel modulations[18] or on non-Newtonian fluid effects.[19,20, 21,22,23,24] In non-Newtonian flows the action of elastic effects and spatially varying shear viscosity on particles come often simultaneously into play, but little is known about the action of a spatially dependent shear viscosity on the particle dynamics alone. We describe in this work a surprising viscosity-gradient driven CSM and the resulting focusing of soft-particles, which occurs even in linear shear flows as indicated in Fig. 1.

Segré and Silberberg found quite early that rigid particles can migrate across straight streamlines to off-center streamline positions in pipe flows [25]. This type of cross-streamline migration (CSM) is inertia driven in the range of intermediate Reynolds number ($\sim 1 < Re <\sim 100$) and it is extensively used for sorting of rigid particles (see e.g. Ref. [5]). In contrast, deformable particles like capsules or cells show CSM already on the scale of microchannels

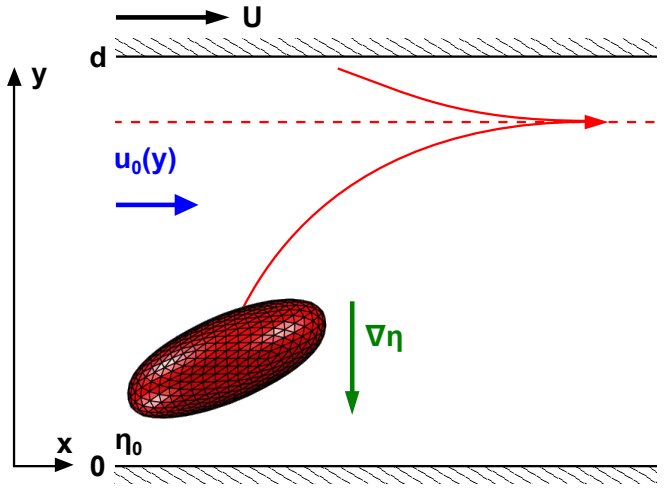

Figure 1. The two solid lines sketch two trajectories of a soft capsule (enlarged) in a shear flow $\mathbf{u}_0(y)$ driven by a moving upper boundary. The shear viscosity of the fluid increases from top to bottom (for instance induced by a temperature gradient) and the capsule migrates towards the region of low viscosity. Along the attractor (dashed line) the migration to a smaller viscosity is in balance with the particle repulsion by the upper boundary.

and in the limit of Stokes flows at very small values of the Reynolds number. The tank-treading motion of vesicles or capsules causes near walls the so-called lift force that drives them away from channel walls in Poiseuille and linear shear flows [7,8,9,10]. Further away from the walls in Poiseuille flows one still has a spatially varying shear rate, which breaks the fore-aft symmetry of deformed particles, so that dumbbells [26,27,28], droplets [11,12], vesicles and capsules [13,14,15,16] exhibit bulk CSM, even in unbounded Poiseuille flows where the interaction with the channel boundaries is neglected. Surprisingly, CSM of soft particles can be driven also by gravitational effects, whereby the migration direction depends on relative directions between the flow and the gravitational force [17]. Migration in Newtonian fluids was also found for non-symmetric soft particles in time-periodic linear shear flows [29] and even shaken liquids when particle inertia is considered [30].

Recent studies of particle CSM use besides Newtonian carrier fluids also visco-elastic fluids. They also break the fore-aft symmetry and may cause already CSM of rigid particles.[24] CSM in viscoelastic liquids is often faster than in Newtonian liquids, which makes non-Newtonian liquids attractive for applications such as in health care or biological and chemical analysis.[19,20,21,22,23,24] Particles in non-Newtonian liquids are sometimes also focused to positions aside of the channel center even in the limit of low Reynolds number flows (see e.g. Ref. [21]). Since in such non-Newtonian liquids shear thinning, leading to a *non-constant viscosity*, comes often simultaneously into play with a fluid elasticity, the specific contribution of a non-constant viscosity to particle CSM is not clear.

Here we study the effects of viscosity gradients on the flow profiles and on the particle dynamics, whereby viscosity gradients may be imposed in a controlled way, for instance, by applying a temperature gradient to fluids [31]. Our modeling approach is described Sec. 2, where also analytical expressions for certain flow profiles and a generalized Oseen tensor are given. In Sec. 3 and Sec. 4 we show by symmetry arguments and numerical simulations, how a viscosity varying perpendicular to the stream lines of a linear shear breaks symmetries and induces CSM of capsules already in simple shear flows, in contrast to liquids with constant viscosity. Two types of viscosity profiles are investigated for plane Poiseuille flows in Sec. 5, where we find also a new scenario for particle stream splitting with interesting applications for particle sorting.

2 Models and Methods

In Sec. 2.1 we consider a constant viscosity gradient perpendicular to the flow lines in linear shear flows and plane Poiseuille flow. We provide for both cases analytical expressions for the flow profile as solutions of the Stokes equation with non-constant viscosity. In Sec. 2.2 we present a generalized Oseen tensor, which takes the first correction of the viscosity gradient into account. It is used in the Stokesian dynamics simulations of the capsule and is derived without the hydrodynamic capsule-wall interactions. The wall effects are taken into account by the Lattice Boltzmann Method described in Sec. 2.3.

2.1 Stokes-flows

We consider fluids between two boundaries located at $y = 0, d$ and a spatially varying viscosity

$$\eta(\mathbf{r}) = \eta_0 + \mathbf{G}_\eta \cdot \mathbf{r} \tag{1}$$

with a constant gradient vector

$$\nabla\eta = \mathbf{G}_\eta \,. \tag{2}$$

We investigate low Reynolds number flows that are determined by the Stokes equation

$$-\nabla p + \nabla \cdot \left\{\eta[\nabla\mathbf{u} + (\nabla\mathbf{u})^{\mathbf{T}}]\right\} = 0 \;, \tag{3}$$

with the pressure p and two choices of boundary conditions at $y = 0, d$.

For a *classical shear cell* with one moving boundary the flow field fulfills the boundary conditions:

$$\mathbf{u}(y=0) = 0 \quad \text{and} \quad \mathbf{u}(y=d) = U\mathbf{e}_x \,. \quad \text{(BC I)} \tag{4}$$

For a pressure driven plane Poiseuille flow with a constant pressure gradient in x-direction, $\nabla p = p_0\mathbf{e}_x$, we use the boundary conditions

$$\mathbf{u}(y=0,d) = 0 \,. \quad \text{(BC II)} \tag{5}$$

If not stated otherwise, we consider further on a viscosity gradient in y-direction

$$\eta(\mathbf{r}) = \eta_0 + G_{\eta,y} y \tag{6}$$

which may be imposed, for instance, by a temperature gradient perpendicular to the two bounding plates. For the viscosity gradient, $G_{\eta,y} \neq 0$, and the solution of the Stokes equation (3) for the boundary conditions BC I gives a nonlinear y-dependence of the velocity in x-direction

$$\mathbf{u}_0(y) = U\frac{\ln[y\,G_{\eta,\mathrm{y}}/\eta_0 + 1]}{\ln[d\,G_{\eta,\mathrm{y}}/\eta_0 + 1]}\mathbf{e}_\mathrm{x} \,. \tag{7}$$

It reduces in the limit $G_{\eta,y} = 0$ to the well known linear shear profile

$$\mathbf{u}_0(y) = U\frac{y}{d}\mathbf{e}_\mathrm{x} \,. \tag{8}$$

For a pressure driven flow between two flat boundaries with the boundary conditions in Eq. (5) the y-dependence of the flow $\mathbf{u}_0(y)$ parallel to the x-axis is given by

$$\mathbf{u}_0(y) = U\frac{Cy - d\ln\left(\frac{G_{\eta,\mathrm{y}}\,y}{\eta_0}+1\right)}{d\left[1+\ln\left(\frac{C\eta_0}{d\,G_{\eta,\mathrm{y}}}\right)\right] - \frac{C\eta_0}{G_{\eta,\mathrm{y}}}}\mathbf{e}_\mathrm{x} \,,$$
$$\text{with} \quad C = \ln\left(\frac{d\,G_{\eta,\mathrm{y}}}{\eta_0}+1\right) \,. \tag{9}$$

This gives in the limit $G_{\eta,y} = 0$ the well known parabolic profile $\mathbf{u}_0(y) = 4Uyd(d-y)\mathbf{e}_x$.

2.2 Stokesian particle dynamics

The surface of the capsule is discretized with N beads at the positions $\mathbf{r}_i$ $(i = 1, \ldots, N)$. Their Stokesian dynamics is described by[32]

$$\dot{\mathbf{r}}_i = \mathbf{u}_0(\mathbf{r}_i) + \sum_{j=1}^{N} \mathbf{H}_{ij} \cdot \mathbf{F}_j \ . \tag{10}$$

The capsule center is given by $\mathbf{r}_\mathrm{c} = \sum_{i=1}^{N} \mathbf{r}_i/N$. The force on bead j is calculated via $\mathbf{F}_j = -\nabla_j V(\mathbf{r})$ with $V(\mathbf{r})$ denoting the total potential (given in the following) and $\mathbf{H}_{ij}$ means the mobility matrix. The mobility matrix is given by

$$\mathbf{H}_{ij} = \begin{cases} \frac{1}{6\pi\eta_i a}\mathbf{1} & \text{if } i = j\,, \\ \mathbf{O}(\mathbf{r}_i, \mathbf{r}_j) & \text{otherwise}\,. \end{cases} \tag{11}$$

with the Oseen tensor $\mathbf{O}$, the Greens function to the Stokes equation (3). For a spatially varying viscosity, i. e. $\mathbf{G}_\eta \neq 0$, we take the leading correction with respect to the small quantity $\frac{(\mathbf{r}_i - \mathbf{r}_j)\cdot\mathbf{G}_\eta}{\eta_j}$ into account

$$\mathbf{O}(\mathbf{r}_i, \mathbf{r}_j) = \frac{1}{8\pi\eta_j R_{i,j}} \left[\left(1 - \frac{\mathbf{R}_{i,j}\cdot\mathbf{G}_\eta}{2\eta_j} \right) \left(\mathbf{1} + \hat{\mathbf{R}}_{i,j}\hat{\mathbf{R}}_{i,j} \right) + \frac{1}{2\eta_j} \left(\mathbf{R}_{i,j}\mathbf{G}_\eta - \mathbf{G}_\eta \mathbf{R}_{i,j} \right) \right] . \tag{12}$$

Herein we use $\eta_j = \eta(\mathbf{r}_j)$, $\mathbf{R}_{i,j} = \mathbf{r}_i - \mathbf{r}_j$, $r_{i,j} = |\mathbf{R}_{i,j}|$ and $\hat{\mathbf{R}}_{i,j} = \frac{\mathbf{R}_{\mathbf{i},\mathbf{j}}}{r_{i,j}}$. A small value of $\frac{(\mathbf{r}_i - \mathbf{r}_j)\cdot\mathbf{G}_\eta}{\eta_j}$ means that the spatial deviation of the viscosity on the size of the capsule is small compared to the local viscosity at the position of the capsule. It can be estimated by the dimensionless number

$$\widetilde{\mathbf{G}}_\eta = \frac{\mathbf{G}_\eta 2R_\mathrm{c}}{\eta_\mathrm{c}} \tag{13}$$

with the viscosity at the center of the capsule $\eta_\mathrm{c} = \eta(\mathbf{r}_\mathrm{c})$ and the capsule's radius R_c. In this form of the Oseen tensor the interaction with the walls is neglected. The derivation of the expression in Eq. (12) is given in SI.

To calculate the forces and the velocity of the capsule on its surface, which is spherical in its equilibrium shape, it must be discretized (see Fig. 1). We begin with a regular icosahedron, which has 12 nodes, and refine the surface iteratively [33]: We add new nodes at the middle of each edge and shift them to the surface of the sphere, until we obtain a good resolution. With this discretization we can calculate the forces at the surface whereby we use an elastic force, a bending force and a penalty force that ensures volume conservation. The elastic force is modeled by the neo-Hookean law that describes a thin plate with a constant surface shear elastic modulus G_s with a potential V_{NH} (for details see Refs. [34,35]). The bending force follows from the potential V_b [36] with $V_b = \frac{\kappa}{2}\sum_{i,j}(1 - \cos\beta_{i,j})$ whereby κ describes the bending stiffness and $\beta_{i,j}$ denotes the angles of the normal vectors between two neighboring triangles. Furthermore we use a penalty force that ensures that the volume is approximately conserved during the simulations [37]. Its potential is given by $V_v = \frac{k_v}{\mathcal{V}_0}(\mathcal{V}(t) - \mathcal{V}_0)^2$ with the instantaneous volume $\mathcal{V}(t)$, the reference volume $\mathcal{V}_0$ and the rigidity k_v. It is useful to measure the capsule's stiffness with a dimensionless number, the capillary number

$$\mathrm{Ca} = \frac{\eta_0 R_\mathrm{c}}{G_s}\dot{\gamma} \tag{14}$$

with (mean) shear rate

$$\dot{\gamma} = \frac{U}{d}\,. \tag{15}$$

If not stated otherwise we use the following parameters for the Stokesian dynamics. Parameters of the flow: d=50, U=0.5, η_0=3, $\mathbf{G}_\eta = 0.03\,\hat{\mathbf{e}}_\mathrm{y}$. Parameters of the capsule: initial position x_0=0, y_0=d/2, z_0=0, forces: k_v=3.0, κ = 0.2, $G_s = 0.2$ (linear shear flow) and $G_s = 0.4$ (Poiseuille flow), mean bead distance $b = 1.0$, Radius $R_\mathrm{c} = 6.6$, bead radius $a = 0.2$, time step $\Delta t = 0.05$. This leads to Ca ≈ 1, $|\widetilde{\mathbf{G}}_\eta| = 0.18$ at the initial position.

A conversion of the parameters to SI units is obtained by multiplying them with:

$$u_\mathrm{m} = 37.88\,\mu\mathrm{m},\ \ u_\mathrm{s} = 1.89\,\mathrm{ms},\ \ u_\mathrm{kg} = 2.39\cdot 10^{-11}\,\mathrm{kg}\,. \tag{16}$$

The radius of the capsule is $R_\mathrm{c} \approx 250\,\mu$m, and the plate distance is $d \approx 2\,$mm. The viscosity of the fluid at the boundaries (if $\mathbf{G}_\eta \parallel -\hat{\mathbf{e}}_\mathrm{y}$) corresponds to water at 20°C with $\eta(y = 0) = 1\,$mPas and 60°C with $\eta(y = d) = 0.5\,$mPas [38,39]. This is a temperature gradient comparable to one discussed in Ref. [31]. The maximal velocity is $U = 1\,$cm / s.

2.3 The lattice-Boltzmann method

To investigate the particle dynamics without the constraint of a small viscosity gradient as for the Stokesian dynamics and in order to take also the effects of the boundaries on particle dynamics into account we use the lattice-Boltzmann method (LBM).

We use a LBM with 19 discrete velocity directions (D3Q19), cf. fig. 2 [40], with the Bhatnagar-Gross-Krook (BGK) collision operator [41,42]. The equation of the probability distribution $f_i(\boldsymbol{r}, t)$ in velocity-direction i at position $\boldsymbol{r}$ is then given by

$$f_i(\boldsymbol{r} + c_i\Delta t, t + \Delta t) = f_i(\boldsymbol{r}, t) - \frac{\Delta t}{\tau}\left(f_i(\boldsymbol{r}, t) - f_i^\mathrm{e}(\boldsymbol{r}, t)\right) + \Delta t F_i\,, \tag{17}$$

whereby τ is a typical relaxation time related to the viscosity of the fluid and F_i contains the external forces[43]. $f_i^\mathrm{e}(\boldsymbol{r}, t)$ is the equilibrium distribution:

$$f_i^\mathrm{e}(\boldsymbol{r}, t) \approx \rho w_i \left[1 + \frac{(\boldsymbol{c}_i\cdot\boldsymbol{u})}{c_\mathrm{s}^2} + \frac{(\boldsymbol{c}_i\cdot\boldsymbol{u})^2}{2c_\mathrm{s}^4} - \frac{u^2}{2c_\mathrm{s}^2} \right] + \mathscr{O}(u^3) \tag{18}$$

with the unit vectors c_i along the discrete directions for the i-th velocity. Furthermore we use the equilibrium fluid density ρ_0, the speed of sound in the LBM-system, $c_\mathrm{s} = \frac{1}{\sqrt{3}}$, and the weighting factors w_i [42].

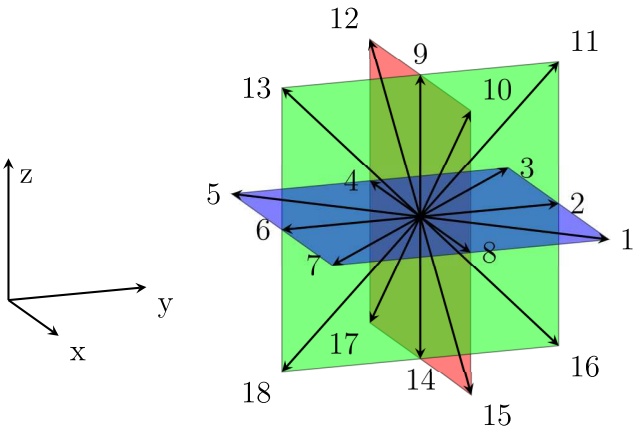

Figure 2. Sketch of the discretized velocity directions of the D3Q19 model for lattice-Boltzmann simulations.

The probability distribution function allows to calculate the density and the velocity of the fluids via

$$\rho(\boldsymbol{r},t) = \sum_i f_i(\boldsymbol{r},t)\,, \tag{19}$$

$$\rho(\boldsymbol{r},t)\boldsymbol{u}(\boldsymbol{r},t) = \sum_i \boldsymbol{c}_i f_i(\boldsymbol{r},t) + \frac{1}{2}\Delta t \boldsymbol{F}(\boldsymbol{r})\,, \tag{20}$$

whereby $\boldsymbol{F}(\boldsymbol{r})$ is the external force density[43]. The viscosity of the fluids is given by

$$\nu(\boldsymbol{r}) = c_\mathrm{s}^2\left(\tau(\boldsymbol{r}) - \frac{1}{2}\right)\Delta t\,. \tag{21}$$

We use a spatial dependent $\tau(\boldsymbol{r})$ to simulate the viscosity gradient given by Eq. (6).

The external forces are coupled to the flow via the immersed boundary method [44]. Thereby one has to consider that the nodes on the membrane of the capsule do not lie on the discrete grid points of the fluid. The force acting on a node of the capsule's surface is distributed to neighbouring fluid nodes with the function $\phi(\Delta\boldsymbol{r}) = \tilde{\phi}(\Delta x)\tilde{\phi}(\Delta y)\tilde{\phi}(\Delta z)$ and

$$\tilde{\phi}(R) = \begin{cases} \frac{1}{4}\left(1+\cos(\frac{\pi R}{2})\right) & \text{if } |R| \le 2 \\ 0 & \text{else} \end{cases}\,. \tag{22}$$

It is also utilized to calculate the velocity at the nodes of the capsule's surface with the velocity of the neighboring fluid nodes. We use periodic boundary conditions in x and z-direction and a standard bounce back scheme at the walls to drive the flow [42].

We use the following parameters for the linear shear flow: Parameters of the flow: density ρ_0=1.0, viscosity $\eta_0 = 1/6$ at $x = 0$, $y = 0$, $z = 0$, viscosity gradient $\mathbf{G}_\eta = 0.002\,\hat{\mathbf{e}}_\mathrm{y}$, velocity of the upper boundary or maximum velocity U=0.005, number of nodes in x-direction N_x=400, number of nodes in z-direction N_z=100, wall distance is $d = 100$. Parameters of the capsule: initial position x_0=0, y_0=51.5 and z_0=49.5, coefficient of the volume preserving force k_v=0.01, bending potential $\kappa = 10^{-4}$, neo-Hookean coefficient $G_\mathrm{s} = 10^{-4}$ node distance $b = 1.0$, which leads to a radius $R = 6.6$, number of nodes $N = 642$ or $R = 13.2$ with $N = 2562$. The time step is $\Delta t = 1.0$. For comparison between LBM and Stokesian dynamics simulations besides the same parameters a bead radius a=0.2 is used.

We use the following parameters for the Poiseuille flow. Parameters of the flow: density ρ_0=1.0, viscosity $\eta_0 = 1/6$ at $x = 0, y = 0, z = 0$, viscosity gradient $|\mathbf{G}_\eta| = 0.009$, velocity of the upper boundary or maximum velocity U=0.15, number of nodes in x-direction N_x=400, number of nodes in z-direction N_z=100, wall distance is $d = 300$. Parameters of the capsule: coefficient of the volume preserving force k_v=0.01, node distance $b = 1.0$ which leads to a Radius $R = 3.3$, number of nodes $N = 162$ or $R = 13.2$ with $N = 2562$, time step $\Delta t = 1.0$, bending potential $\kappa = 0.17$ (large R), bending potential $\kappa = 0.02$ (small R), neo-Hookean coefficient $G_\mathrm{s} = 10^{-3}$ (large R), neo-Hookean coefficient $G_\mathrm{s} = 5 \times 10^{-4}$ (small R).

3 Explanation of $\nabla\eta$-induced CSM

We develop at first a qualitative explanation of the CSM induced by a viscosity gradient perpendicular to stream lines. A viscosity gradient modifies the flow profiles as indicated in Eq. (7) and Eq. (9), i.e. the shear rate across the particle is not constant but is slightly varying. This variation of the shear rate is neglected for the qualitative explanation here. We show that the CSM is directly caused by the $\nabla\eta$-induced modifications of the friction forces acting on the particle's surface and not indirectly by the varying shear rate (this is also confirmed by simulations, cf. SI).

We consider at first a spherical capsule. Without a viscosity gradient, the capsule rotates due to the linear shear flow (see Eq. (8) and Fig. 3 (a)) and its center $\mathbf{r}_\mathrm{c}$ follows a flow line. [32,16,13] The velocity at the capsule's surface in the comoving frame is given by $\tilde{\mathbf{u}}_\mathrm{s}(\tilde{\mathbf{r}}) = \boldsymbol{\omega} \times \tilde{\mathbf{r}}$ with $\tilde{\mathbf{r}} = \mathbf{r} - \mathbf{r}_\mathrm{c}$, $\boldsymbol{\omega} = \frac{1}{2}\nabla \times \mathbf{u}_0$ and the shear flow in the comoving frame $\tilde{\mathbf{u}}_0(\tilde{y}) = U\tilde{y}/d\mathbf{e}_\mathrm{x}$. The friction forces $\mathbf{F}(\tilde{\mathbf{r}})$ between the capsule and the fluid can be calculated by solving Eq. (10) for the forces $\mathbf{F}_j = \mathbf{F}(\tilde{\mathbf{r}}_j)$. In the following we show how this friction force is affected if this rotation is performed in the presence of a viscosity gradient.

A spherical capsule in a linear shear flow without viscosity gradient has symmetries: The spherical capsule is invariant under a reflection at the $\tilde{x}\tilde{z}$- or $\tilde{y}\tilde{z}$-plane. Also the flow's magnitude is equal after these reflections, but the flow changes its sign, cf. Fig. 3 (a). Therefore the velocity and the friction at the surface of the capsule have the same symmetries: At the mirrored position $\tilde{\mathbf{r}}'$ of $\tilde{\mathbf{r}}$ at the $\tilde{x}\tilde{z}$-plane we get $F_\mathrm{x}(\tilde{\mathbf{r}}') = -F_\mathrm{x}(\tilde{\mathbf{r}})$ and $F_\mathrm{y}(\tilde{\mathbf{r}}') = F_\mathrm{y}(\tilde{\mathbf{r}})$ (analogously at the $\tilde{y}\tilde{z}$-plane). The direction of the friction forces from the fluid on the capsule is indicated in Fig. 3

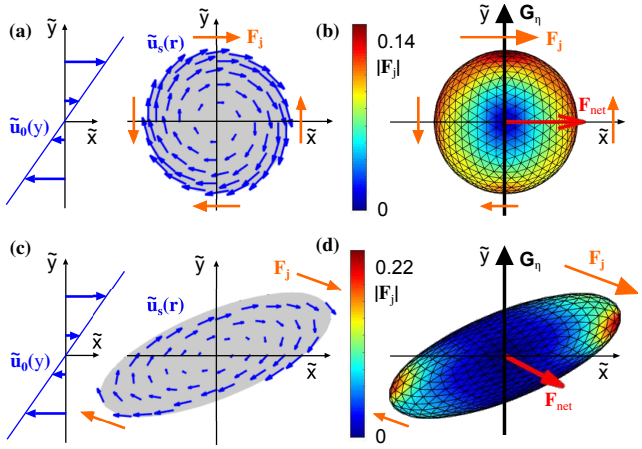

Figure 3. A rigid capsule is rotating due to the shear flow $\tilde{\mathbf{u}}_0(y)$ with velocity $\tilde{\mathbf{u}}_s(\mathbf{r})$ at its surface (comoving frame, without gradient) (a). This leads to friction forces $\mathbf{F}(\tilde{\mathbf{r}})$ (orange arrows), but the sum of these forces is zero because of the symmetry to the $\tilde{x}\tilde{z}$- and $\tilde{y}\tilde{z}$-plane. This motion in presence of a viscosity gradient $\mathbf{G}_\eta \parallel \hat{\mathbf{e}}_y$ (black) leads to higher friction forces on one half than on the other (orange arrows and color of surface) (b). This asymmetry causes a net force $\mathbf{F}_{\text{net}}$ (red) which is oriented in flow direction, i.e. it causes no CSM. A soft capsule is deformed and performs a tank-treading motion (c) in a linear shear flow (shown without a gradient). Due to its ellipsoidal shape it is not symmetric to the $\tilde{x}\tilde{z}$- and $\tilde{y}\tilde{z}$-plane, but has a point symmetry that prevents a net force. A gradient (d) breaks the point symmetry and leads to a net force with a component perpendicular to the flow. This results in a CSM towards regions with a lower viscosity.

(a). As example at the point of the capsule with the highest y-value the friction force points in positive x-direction and at the point with the lowest y-value the force points in negative x-direction and has the same magnitude. This symmetry determines the net force via

$$\begin{aligned} F_{\text{net,x}} &= \oint F_{\text{x}} dA = \int_{y>y_{\text{c}}} F_{\text{x}} dA + \int_{y<y_{\text{c}}} F_{\text{x}} dA \\ &= \int_{y>y_{\text{c}}} F_{\text{x}} dA - \int_{y>y_{\text{c}}} F_{\text{x}} dA = 0\,, \end{aligned} \tag{23}$$

$$\begin{aligned} F_{\text{net,y}} &= \oint F_{\text{y}} dA = \int_{x>x_{\text{c}}} F_{\text{y}} dA + \int_{x<x_{\text{c}}} F_{\text{y}} dA \\ &= \int_{x>x_{\text{c}}} F_{\text{y}} dA - \int_{x>x_{\text{c}}} F_{\text{y}} dA = 0\,, \end{aligned} \tag{24}$$

whereby $\int_{y>y_{\text{c}}} dA$ denotes an integration over the half sphere on the side of the xz-plane with $y > y_{\text{c}}$. The symmetries show that the force on one half of the sphere has the opposite direction of the force on the other half. Thus the net forces is zero for a constant viscosity. Furthermore the system is symmetric to the $\tilde{x}\tilde{y}$-plane which prevents a force in z-direction:

$$F_{\text{net,z}} = 0\,. \tag{25}$$

We discuss now the effect of a viscosity gradient oriented perpendicular to the flow direction and in the shear plane, i. e. $\mathbf{G}_\eta \parallel \hat{\mathbf{e}}_y$ as shown in Fig. 3 (b). With the viscosity gradient the friction at the upper half of a rigid spherical capsule ($y > y_{\text{c}}$), which is directed in positive x-direction, is higher due to the higher viscosity than at the lower half ($y < y_{\text{c}}$), which is directed in negative x-direction. Because the magnitude of the friction is not equal at both halves the symmetry used to derive Eq. (23) is broken. Thus a net force is caused by the rotation in presence of the viscosity gradient, even in a linear shear flow.

But the magnitude of the friction still has a symmetry to the $\tilde{y}\tilde{z}$-plane. This can be seen with Fig. 3 (b) by comparing the left part of the capsule ($x < x_{\text{c}}$) and the right part ($x > x_{\text{c}}$). Both halves are symmetric because the viscosity increases in y-direction and not in x-direction. Thus the symmetry used in Eq. (23) is broken, but eqs. (24) and (25) are still valid. Therefore, the net force is oriented in x-direction, i.e. $\mathbf{F}_{\text{net}}$ is parallel to the flow. Thus a rigid sphere shows migration along the flow direction but no CSM. The effects of further possible directions of the viscosity gradient on rigid particles are discussed in SI.

The behavior of a deformable capsule is different. Its tank-treading motion and shape obtained by simulations in a linear shear flow without a viscosity gradient is shown by Fig. 3 (c). The capsule adopts an ellipsoidal shape with its major axis inclined with respect to the flow direction. The capsule's center follows the flow direction. The friction forces are calculated in the same way as for a rigid capsule. The main difference to the rigid capsule is the ellipsoidal shape, which has no mirror symmetries with respect to the $\tilde{x}\tilde{z}$- and $\tilde{y}\tilde{z}$-plane. But the deformed shape and the shear flow have both a point symmetry to the capsules center (see Fig. 3 (c)) and a symmetry to the $\tilde{x}\tilde{y}$-plane. The friction force has the same symmetry. As example the friction force at two points is shown in Fig. 3 (c). At the points with the highest y-value the friction force from the flow on the ellipsoidal, tank-trading particle points in positive x- and negative y-direction. At the mirrored points with the lowest y-value the force points in negative x- and positive y-direction. Thus eqs. (23), (24) and (25) can also be used in case of a deformable capsule, which means $\mathbf{F}_{\text{net}} = 0$ for a constant viscosity.

We discuss now the effect of a viscosity gradient perpendicular to the flow direction and in the shear plane $\mathbf{G}_\eta \parallel \hat{\mathbf{e}}_y$ (other orientations: see SI). The symmetry with respect to the center is broken and eqs. (23) and (24) are not valid in this case. This is shown in Fig. 3 (d): The force at the point with the highest y-value at the high viscosity, which points in positive x- and negative y-direction, has a higher magnitude than the mirrored force. This leads to a non-zero net force $\mathbf{F}_{\text{net}}$ which is oriented in positive x- and negative y-direction. The system still has a symmetry to the $\tilde{x}\tilde{y}$-plane, so that Eq. (25) is still valid and the net force has no z-component. The negative y-component of the net force leads to a CSM towards the lower viscosity. Note that this is different to the rigid capsule, whose symmetry to the $\tilde{y}\tilde{z}$-plane prevents a force in y-direction. Thus a CSM due to a viscosity gradient is found only if the capsule is soft.

4 CSM in a shear flow

Here we confirm by simulations the qualitative reasoning described in the previous section, that a finite viscosity gradient, $\nabla\eta$, causes a CSM of deformable particles already in simple shear flows. We use a generalized Oseen tensor given by Eq. (12), which takes the leading order effects of $\nabla\eta$ into account, and determine in Stokesian-dynamics simulations the capsule's CSM velocity as function of parameters. By LBM simulations of a capsule we evaluate the validity range of these approximate results and we show that capsules in shear flows with $\nabla\eta \neq 0$ are focused to an attractor streamline.

4.1 Numerical results on $\nabla\eta$-induced bulk migration

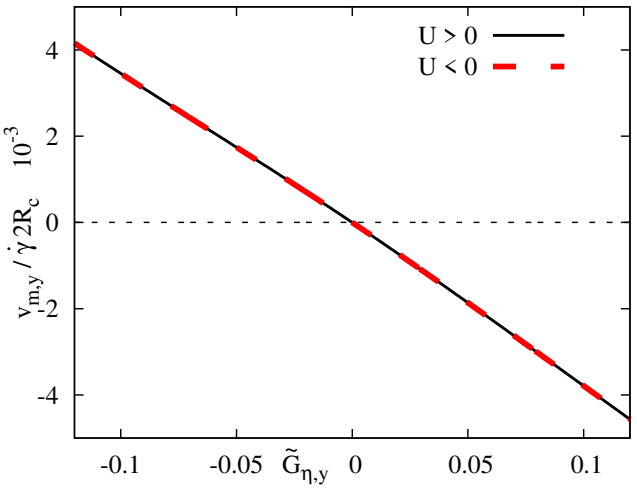

Figure 4. The migration velocity $v_{m,y}$ in units of $2\dot{\gamma}R_c$ as function of the dimensionless viscosity gradient $\tilde{G}_{\eta,y}$. The CSM is directed towards the lower viscosity as sketched in Fig. 3 and it is independent of the sign of U, i. e. independent of the flow direction.

In Stokesian dynamics simulations we use the nonlinear shear flow profile given by Eq. (7) and the generalized Oseen tensor given in Eq. (12). We simulate trajectories $y_c(t)$ of the capsule and determine by linear fits to the slope of capsule trajectories $y_c(t)$ the cross-stream migration velocity $v_{m,y}$. The resulting $v_{m,y}$ of capsules is shown in Fig. 4 as function of the dimensionless viscosity gradient $\widetilde{\mathrm{G}}_{\eta,\mathrm{y}}$. The CSM velocity in Fig. 4 decreases nearly linearly with $|\widetilde{\mathrm{G}}_{\eta,\mathrm{y}}|$ and is oriented as explained in the previous section, cf. Fig. 3. In addition, the migration is directed towards the lower viscosity and does not depend on the flow's direction, i.e. it is independent on the sign of U. The nonlinear y-dependence of the flow velocity in Eq. (7) and therefore the spatially varying velocity gradient causes in Fig. 4 only a slight deviation of v_{m_y} from a linear dependence on $\widetilde{\mathbf{G}}_\eta$ at small values of $|\widetilde{\mathrm{G}}_{\eta,\mathrm{y}}|$ (a more detailed comparison of the CSM in both flow profiles is given in the SI). This justifies the assumption of a constant velocity gradient across the capsule used in the previous section 3.

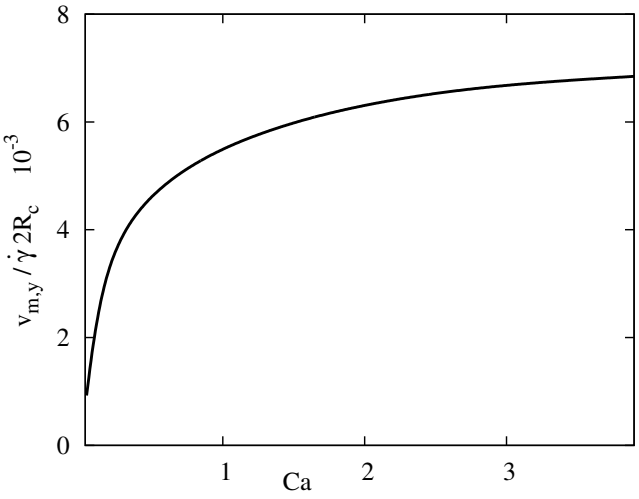

Figure 5. The migration velocity $v_{m,y}$ is given in units of $2\dot{\gamma}R_c$ and as function of the capillary number Ca given by Eq. (14). The migration vanishes at a high capsule-stiffness $\mathrm{Ca} \ll 1$ and increases with Ca.

Fig. 5 shows the dependence of the migration velocity on the stiffness of the capsule: The CSM decreases with increasing stiffness and vanishes at small values of the capillary number $\mathrm{Ca} \ll 1$ given in Eq. (14). This underlines the importance of the deformability of particles for their cross streamline migration (see also Fig. 3).

The generalized Oseen tensor in Eq. (12) takes into account the first order correction with respect to the viscosity gradient, i.e. it is valid for small values of $|\widetilde{\mathbf{G}}_\eta|$. To estimate the validity range of this approximation we compare the CSM velocity $v_{m,y}$ as obtained by Stokesian dynamics simulations using the generalized Oseen tensor in Eq. (12) with that obtained by Lattice-Boltzmann simulations of capsules. In order to keep in LBM simulations the interaction of the capsule with the boundary small, we positioned it in the middle of the flow cell between the two boundaries. In addition we have chosen a small ratio between the capsule's diameter and the wall distance $\frac{2R_c}{d} \approx 0.13$. Furthermore a sufficiently small Reynolds number $\mathrm{Re}=\frac{\rho U R_c}{\eta_0} \approx 0.2$ was chosen in LBM simulations to match the low Reynolds number regime of the Stokesian dynamics simulations. The flow is simulated for the boundary condition given by Eq. (4) and the viscosity gradient points into the direction perpendicular to the boundaries.

The migration velocities resulting from both simulations are shown in Fig. 6. The simulation results for the capsule with the generalized Oseen tensor and those obtained via the LBM agree well in the range of small values of $|\widetilde{\mathbf{G}}_\eta|$ and the deviation increases with $|\widetilde{\mathbf{G}}_\eta|$. For example at $|\widetilde{\mathbf{G}}_\eta| \lessapprox 0.15$ the relative error is below 10% and at $|\widetilde{\mathbf{G}}_\eta| \lessapprox 0.18$ the error is below 20%.

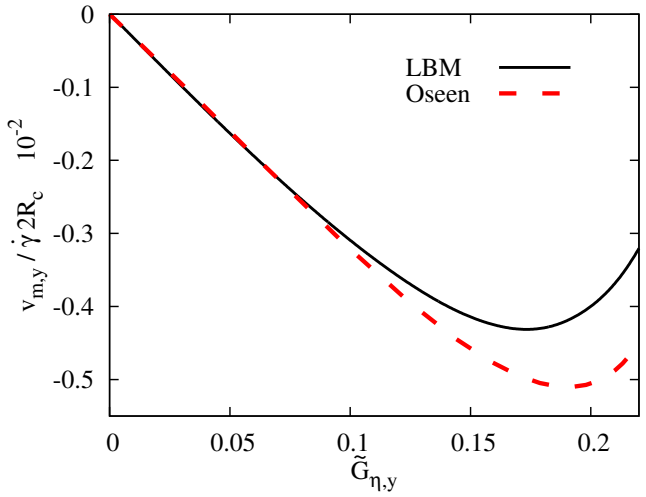

Figure 6. The CSM velocity $v_{m,y}$ is determined by Stokesian dynamics simulations (dashed) and by Lattice-Boltzmann simulations (solid). The expansion up to leading order of the viscosity gradient $\tilde{G}_\eta$, as used in Stokesian dynamics simulations, leads for $v_{m,y}$ to an error less than 10% if $|\tilde{\mathbf{G}}_\eta| \lessapprox 0.15$ compared to the LBM.

4.2 Particle focusing to an attractor streamline

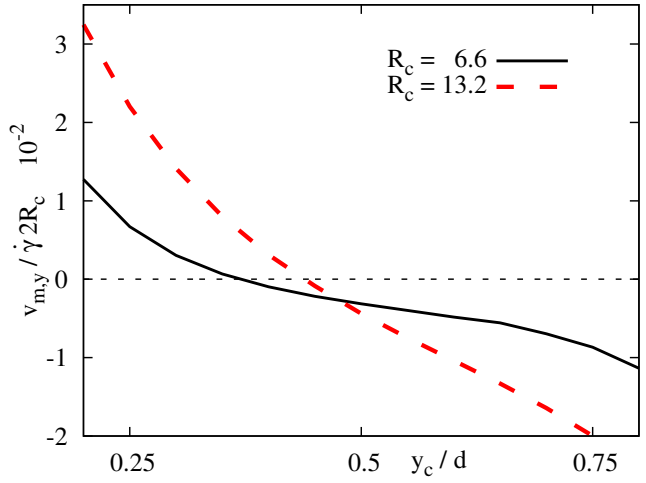

Figure 7. The migration velocity of a soft capsule in a flow with viscosity gradient and the boundary conditions in Eq. (4) is determined by the LBM as function of the initial position y_c for two different particle radii R_c. Far away from the walls the particle migrates due to the viscosity gradient towards the lower viscosity, i.e. towards the plate at $y = 0$. Close to the walls the repulsive wall interaction dominates, which leads to a migration away from the walls. Hence there is a stable position, i.e. an attractor off center, that depends on the particle's size. It is located at $y \approx 0.37d$ with $2R_c/d = 0.13$ and at $y \approx 0.41d$ with $2R_c/d = 0.26$.

The LBM includes the hydrodynamic interaction of the capsule with the walls, which causes a so-called lift force that repels the capsule from walls and that depends on the capsule-wall distance [7,8,9]. The interplay with the lift force causes a y-dependent migration velocity as shown for two capsules with two different radii in Fig. 7. The dimensionless gradient ranges in this case from $G_y = 0.16$ (at $y = 0$) to $\tilde{G}_y = 0.07$ ($y = d$) with $R_c = 6.6$ and with $R_c = 13.6$ from $\tilde{G}_y = 0.14$ to $\tilde{G}_y = 0.32$. The CSM caused by $\nabla\eta$ and the wall repulsion balance each other in the range of the lower viscosity and at this value of y the migration velocity $v_{m,y}$ vanishes. The location of this attractor position depends on the capsule size. We find the attractor at $y \approx 0.37d$ for $2R_c/d = 0.13$ and $y \approx 0.41d$ for $2R_c/d = 0.26$.

5 Simulation of CSM in Poiseuille flow

Capsules and red blood cells migrate in a Poiseuille flow, driven by the spatial varying shear gradient across a soft particle, usually to the center of the flow channel. [13,14, 15,16] If one has a viscosity gradient perpendicular to the boundaries across a plane Poiseuille flow, the $\nabla\eta$ induced migration has in the whole cell the same direction i. e. the $\nabla\eta$ induced migration either supports or acts against the common center directed migration. This interplay is investigated by Stokesian dynamics simulation in unbounded (bulk) Poiseuille flows and by LBM simulations, where boundary effects are included.

If a constant $\nabla\eta$ is used, e.g. induced by a temperature gradient across the flow, then the maximal velocity of a Poiseuille flow is shifted towards the lower viscosity. We study here the migration in such a flow profile. However, also with shear thinning fluids a viscosity gradient can be generated. It is well known from shear thinning fluids, that the viscosity has its maximum in the center of a Poiseuille flow and decreases towards the walls. Particle migration is recently studied also in Non-Newtonian fluids, whereby in these works besides shear-thinning effects also elastic effects are considered to be important. In order to contribute to the understanding of CSM of soft particles in shear thinning fluids, we mimic also shear thinning fluids by studying the effects of a viscosity on the migration behavior of a capsule, where the viscosity has its maximum in the channel center and decays linearly to the boundaries.

5.1 Migration in *unbounded* Poiseuille flow induced by $\nabla\eta = const.$

Here we consider as in the previous section a capsule in a fluid with constant viscosity gradient along the y-axis (e.g. generated by a temperature gradient) given by Eq. (6) but now with a Poiseuille flow profile given by Eq. (9). We simulate the capsule's Stokesian dynamics by using the generalized Oseen tensor given in Eq. (12). With the flow profile in Eq. (9) the simulations focus on the behavior of the capsule in the bulk of a Poiseuille flow, where the hydrodynamic interactions between the capsule and the wall are negligible. This allows a direct comparison between the well known bulk CSM in Poiseuille flow (see e.g. Refs. [14,16]) and the $\nabla\eta$ induced CSM.

Figure 8 shows the migration velocity of the capsule as function of its y position with and without a viscosity gradient. For $\widetilde{G}_{\eta,y} = 0$ the capsule migrates to the center and the related CSM velocity $v_{m,y}$ is indicated by the dashed line.

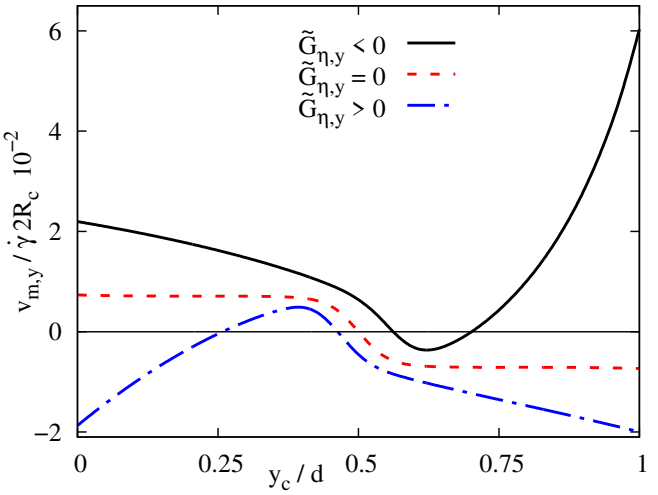

Figure 8. The migration velocity $v_{m,y}/(2\dot{\gamma}R_c)$ of a capsule in the distorted Poiseuille flow profile given by Eq. (9) is shown. It is obtained by Stokesian dynamics simulation as function of the capsule position y/d. The CSM is calculated for two viscosity gradients, one pointing to negative and the other into the positive y-direction as well as with a vanishing viscosity gradient. Without a gradient the capsule migrates towards the center as expected (see e.g. Refs. [14,16]). In the case of a viscosity gradient the capsule migrates again towards the lower viscosity, besides a small region close to the center, where the shear rate of the flow profile in Eq. (9) vanishes.

With a gradient in negative y-direction, i.e. $\widetilde{G}_{\eta,y} < 0$, the viscosity ranges from $\eta(y=0) = 3$ to $\eta(y=d) = 1.5$. The CSM velocity for this case is given by the solid line in Fig. 8. The $\nabla\eta$ effect enhances in a range of smaller y the CSM velocity to the center, i.e. in positive y-direction. Near the channel center at $y = 0.54d$ the flow has its maximal velocity and the shear rate of the flow field given by Eq. (9) vanishes. At this position the $\nabla\eta$ induced migration vanishes too and the migration directed to the channel center dominates. Thus capsules with an initial position $y_0 \lessapprox 0.7\,d$ migrate until they reach the attractor near the center. At initial positions $y_0 \gtrapprox 0.7\,d$ the $\nabla\eta$ induced outward migration dominates and the capsules migrate away from the center. This outward migration is near $y = d$ approximately up to 8 times faster than the center oriented one.

With a gradient in positive y-direction the viscosity ranges from $\eta(y=0) = 3$ to $\eta(y=d) = 4.5$. The situation is similar and the migration is also directed to the region of the lower viscosity, which is now located at the plate at $y = 0$. Therefore we get $v_{m,y} < 0$ again besides the region close to the center. Capsules with an initial position $y_0 \gtrapprox 0.25\,d$ migrate to the attractor close to the center at $y = 0.44\,d$ and capsules with $y_0 \lessapprox 0.25\,d$ migrate to the wall at $y = 0$.

5.2 Migration in *bounded* Poiseuille flow induced by $\nabla\eta = const.$

Here we describe results of LBM simulations of a capsule for $\nabla\eta = const.$ and the flow field boundary conditions given in Eq. (5). Figure 9 (a) shows the spatial dependence of the flow velocity and the linear increase of the viscosity. This demonstrates that the maximum flow velocity in Poiseuille flow is shifted towards the lower viscosity.

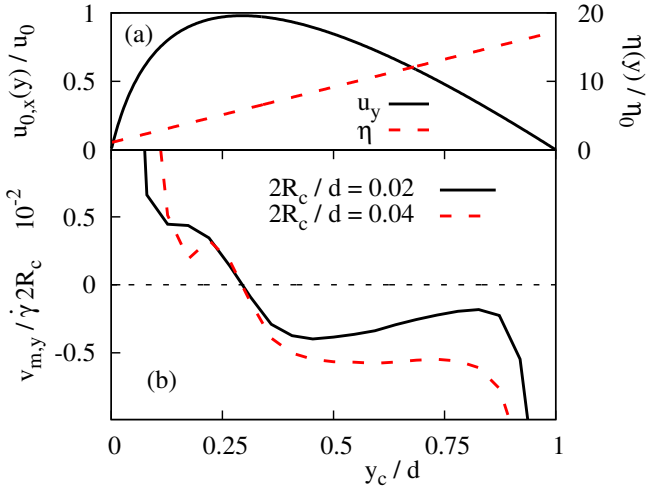

Figure 9. (a) The spatial dependence of the flow velocity $u_{0,x}(y)$ (solid line) and the viscosity for a linear increase of the viscosity between both boundaries (dashed line). The maximal velocity is shifted towards the region with the lower viscosity. (b) The spatial dependence of the migration velocity with wall interaction for two different capsule radii R_c. The attractor with vanishing $v_{m,y}$ is shifted towards the lower viscosity due to the shift of the maximal flow velocity.

The Fig. 9 (b) shows the migration velocity $v_{m,y}$ as function of y_c/d. In contrast to the case without wall interaction (cf. Fig. 8) only the attractor at the maximal flow velocity and no repeller is found. The reason is that wall induced repelling lift force is stronger than the $\nabla\eta$ induced migration to large values of y, even at higher values of $\tilde{G}_y$. The shift of the attractor with $v_{m,y} = 0$ to smaller values of y than the channel center has its origin in the shift of the maximal flow velocity to smaller values of y. Hence, in the presence of walls the capsule migrates always to one attractor that is shifted away from the flow center by the constant viscosity gradient. However, the migration velocity is larger in the presence of the viscosity gradient.

5.3 Particle attractor splitting induced by $\nabla\eta \neq const.$

Here we study the capsules dynamics by LBM simulations in a viscosity profile that is maximal at the channel center and decreases linearly towards the walls, as indicated by the dashed line in Fig. 10 (a). A decay of the shear viscosity in Poiseuille flow is known for shear thinning fluids and the viscosity profile in Fig. 10 (a) is a very simple mimicry

of the shear viscosity of shear thinning fluids. For this viscosity profile one obtains in simulations a Poiseuille flow profile, cf. solid line in Fig. 10 (a), which is flattened near the channel center similar as for shear thinning fluids.

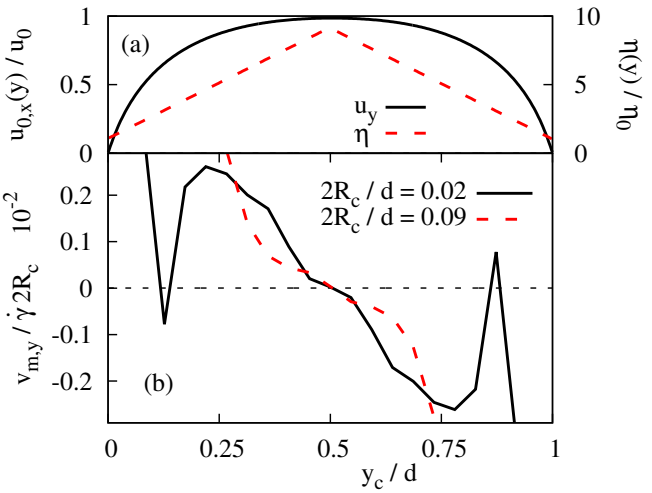

Figure 10. (a) The spatial variations of the shear viscosity (dashed line) and the flattened velocity profile $u_{0,x}(y)$ (solid line). (b) The y-dependence of migration velocity as obtained by LBM simulations of a capsule for two different radii. For the smaller particle radius a second attractor emerges.

The migration velocity of capsules in this viscosity profile is shown in Fig. 10 (b) for two different radii of the capsule. The attractor at the channel center is not shifted by this viscosity profile, because the shear rate vanishes at the channel center and the $\nabla\eta$ induced migration as well. In this region close to the center the center directed migration dominates. However, for the smaller capsule with $2R_c/d = 0.02$ the migration velocity, represented by the solid line in Fig. 10 (b), changes on each side of the channel center two times its sign. At the outer zero of $v_{m,y}$ an additional particle attractor has emerged. It is caused, similar as for the linear shear flow in the previous section 4.2, by the interplay between outward directed $\nabla\eta$ induced migration, which outweighs here the center directed migration, and the wall repulsion. This is similar also to the unbounded flow, where the outward directed $\nabla\eta$ induced migration can overcome the center migration (cf. Fig. 8). Between two neighboring attractors the vanishing migration velocity $v_{m,y}$ marks a particle repeller.

The emergence of the off-center attractors enables interesting applications. If in a viscosity profile, similar as in Fig. 10 (a), particles of different sizes are injected near one boundary, the larger ones migrate to the attractor at the channel center and the smaller ones may stay along the off-center attractor. I. e. at the end of the channel particles of different size or elasticity (cf. Fig. 3 and Fig. 5) are separated. This is a interesting new concept in microfluidics for the separation of different soft particles.

In investigations with viscoelastic fluids a particle migration to off-center attractors has been reported before [19,20,21,22,23,24] and it is not always clear whether this type of migration is driven more by elastic or viscosity effects. Here the mechanisms of an outward directed migration to an off-center attractor, driven by the $\nabla\eta$ effects, are rather clear. Therefore, our model with the viscosity profile shown Fig. 10 (a), may help for an improved understanding of CSM in viscoelastic fluids.

6 Discussion and conclusions

We investigated the effects of a spatially varying viscosity on the flow profile in shear and Poiseuille flow and we described a novel viscosity-gradient driven cross-streamline migration (CSM) of soft capsules, which represents deformable particles. A viscosity gradient in microfluidic devices may be induced, for instance, by a temperature gradient [31].

For the Stokesian dynamics simulations of capsules we determined flow profiles that take a constant viscosity gradient into account. We also derived for these simulations a generalized Oseen tensor that includes the viscosity gradient. These results may be also utilized in other approaches such as the boundary integral method [45] or in simulations of microswimmers [46], polymers [47] and colloids [32].

Rigid and soft particles in liquids of constant viscosity do not migrate across the streamlines in linear shear flows [16]. We have shown by symmetry arguments how the interplay between the particle deformability and the Stokes-friction forces, that vary according to a viscosity gradient across a particle, leads to cross-streamline migration of deformable capsules in simple shear flows towards the region of lower viscosity. This reasoning may also apply to the particle dynamics in non-Newtonian fluid flows, whereby in this case often elastic effects have to be taken into account as well. Our prediction on the basis of symmetry arguments are confirmed by Stokesian dynamics simulations. By Lattice Boltzmann simulations, where the particle wall interactions are taken into account, we also show that the interplay between this viscosity-gradient induced migration and the hydrodynamic wall repulsion causes even in linear shear flows a focusing of particles to an attractor streamline in the low viscosity region as indicated in Fig. 1. The location of the attractor depends on the strength of the viscosity gradient and the particle properties. This predicted focusing may have interesting applications.

We investigated CSM also in Poiseuille flows for two different viscosity gradients. A constant viscosity gradient across plane Poiseuille flow may be induced again by a temperature gradient across a flow cell. CSM in the presence of a viscosity gradient is much faster than without a gradient. As example we showed that the viscosity gradient, that corresponds to water with a temperature difference of 40°C between the boundaries at a distance of 2 mm, can already enhance the migration velocity by up to a factor 8. Such gradients are reported from experiments [31], also higher viscosity gradients can be achieved with e.g. sucrose in water [48]. Besides the faster migration, also the location of the particle attractor in Poiseuille flow is

affected by the viscosity gradient: It is shifted away from the center of a Poiseuille flow. The major reason for this shift is, that the location of the maximum of flow profile and therefore the position of zero shear rate is shifted towards the region of lower viscosity, which also shifts the position of the attractor. Thus the location of the particle attractor can be controlled by the viscosity gradient in a Poiseuille flow as well.

Shear thinning fluids in Poiseuille flows display a variation of the viscosity gradient with a maximum of the viscosity at the channel center. We described the viscosity landscape of shear thinning fluids in a simplified manner. At the channel center we also have chosen the viscosity maximum and a linear decay towards the channel boundaries. In order to focus to the effects of viscosity gradients, we have neglected further possible effects in complex fluids, such as elastic forces. The assumed viscosity landscape changed the CSM velocity as function of the distance from channel center considerably, compared to fluids with constant viscosity. Moreover, the CSM induced by stronger viscosity gradients dominates and drives in a larger off-center region of the channel cross section particles towards the boundaries. In this range the interplay with particle-wall repulsion may even cause, besides the particle attractor at the channel center, two further off-center particle attractors. These attractors are found for smaller but not for larger soft particles. A similar behavior was also found in experiments with visco-elastic liquids [24,21]. Here we can identify the appearance of off-center particle attractors in a unique manner with the viscosity gradient. Our insights may contribute to a further understanding of cross-streamline migration in complex liquids in straight and possibly in wavy channels [18].

The support by the German French University (DFH/UFA) and discussion with A. Förtsch, D. Kienle and W. Schmidt are gratefully acknowledged.

Author contribution statement

ML and WZ designed the research; ML performed the calculations and the simulations; ML and WZ interpreted and discussed the results and wrote the paper.

References

1. T. M. Squires and S. R. Quake, Rev. Mod. Phys. **77**, 978 (2005).
2. A. S. Popel and P. C. Johnson, Annu. Rev. Fluid Mech. **37**, 43 (2005).
3. A. Karimi, S. Yazdi, and A. M. Ardekani, Biomicrofluidics **7**, 021501 (2013).
4. J. B. Dahl, J.-M. G. Lin, S. J. Muller, and S. Kumar, Ann. Rev. Chem. Biomol. Eng. **6**, 293 (2015).
5. H. Amini, W. Lee, and D. D. Carlo, Lap Chip **14**, 2739 (2014).
6. T. W. Secomb, Annu. Rev. Fluid Mech. **49**, 443 (2017).
7. I. Cantat and C. Misbah, Phys. Rev. Lett. **83**, 880 (1999).
8. U. Seifert, Phys. Rev. Lett. **83**, 876 (1999).
9. M. Abkarian, C. Lartigue, and A. Viallat, Phys. Rev. Lett. **88**, 068102 (2002).
10. X. Grandchamp *et al.*, Phys. Rev. Lett. **110**, 108101 (2013).
11. L. G. Leal, Annu. Rev. Fluid Mech. **12**, 435 (1980).
12. S. Mandal, A. Bandopadhyay, and S. Chakraborty, Phys. Rev. E **92**, 023002 (2015).
13. A. Helmy and D. Barthès-Biesel, J. Mecanique theorique appliquee **1**, 859 (1982).
14. B. Kaoui *et al.*, Phys. Rev. E **77**, 021903 (2008).
15. G. Coupier, B. Kaoui, T. Podgorski, and C. Misbah, Phys. Fluids **20**, 111702 (2008).
16. S. K. Doddi and P. Bagchi, Int. J. Multiphas. Flow **34**, 966 (2008).
17. A. Förtsch, M. Laumann, D. Kienle, and W. Zimmermann, EPL **119**, 64003 (2017).
18. M. Schlenk *et al.*, Lab Chip **18**, 3163 (2018).
19. G. D'Avino *et al.*, Comput. Fluids **39**, 709 (2010).
20. D. Yuan *et al.*, Lab Chip **18**, 551 (2018).
21. F. Del Giudice, S. Sathish, G. D'Avino, and A. Q. Shen, Anal. Chem. **89**, 13146 (2017).
22. X. Lu, C. Liu, G. Hu, and X. Xuan, J. Colloid. Interf. Sci. **500**, 182 (2017).
23. M. A. Faridi *et al.*, J. Nanobiotechnol. **15**, 3 (2017).
24. G. D'Avino, F. Greco, and P. L. Maffettone, Annu. Rev. Fluid Mech. **49**, 341 (2017).
25. G. Segré and A. Silberberg, Nature **189**, 209 (1961).
26. G. Sekhon, R. Armstrong, and M. S. Jhon, J. Polymer Sci.:Polymer Phys. **20**, 947 (1982).
27. P. O. Brunn, Int. J. Multiphase Flow **187**, 202 (1983).
28. M. S. Jhon and K. F. Freed, J. Polymer Sci.: Polymer Phys. **23**, 255 (1985).
29. M. Laumann *et al.*, EPL **117**, 44001 (2017).
30. I. Jo, Y. Huang, W. Zimmermann, and E. Kanso, Phys. Rev. E **94**, 063116 (2016).
31. V. Miralles, A. Huerre, F. Malloggi, and M.-C. Jullien, Diagnostics **3**, 33 (2013).
32. J. K. G. Dhont, *An Introduction to dynamics of colloids* (Elsevier, Amsterdam, 1996).
33. T. Krueger, F. Varnik, and D. Raabe, Comput. Math. Appl. **61**, 3485 (2011), mesoscopic Methods for Engineering and Science Proceedings of ICMMES-09.
34. S. Ramanujan and C. Pozrikidis, J. Fluid. Mech. **361**, 117 (1998).
35. D. Barthès-Biesel, Annu. Rev. Fluid Mech. **48**, 25 (2016).
36. G. Gompper and D.M. Kroll, J. Phys. I France **6**, 1305 (1996).
37. T. Krueger, M. Gross, D. Raabe, and F. Varnik, Soft Matter **9**, 9008 (2013).
38. J. Kestin and J. Shankland, J. Non-Equil. Thermody. **6**, 241 (2009).
39. S. Gupta, *Viscosity of Water. In: Viscometry for Liquids* (Springer Series in Materials Science, Cham, 2014).
40. T. Krüger *et al.*, *The Lattice Boltzmann Method - Principles and Practice* (Springer, Berlin, 2016).
41. P. L. Bhatnagar, E. P. Gross, and M. Krook, Phys. Rev. **94**, 511 (1954).
42. C. K. Aidun and J. R. Clausen, Annu. Rev. Fluid. Mech **42**, 439 (2010).
43. Z. Guo, C. Zheng, and B. Shi, Phys. Rev. E **65**, 046308 (2002).
44. C. S. Peskin, Acta Numer. **11**, 479 (2002).

45. C. Pozrikidis, *Boundary Integral and Singularity Methods for Linearized Viscous Flow* (Cambridge University Press, Cambridge, England, 1992).
46. J. Elgeti, R. G. Winkler, and G. Gompper, Rep. Prog. Phys. **78**, 056601 (2015).
47. M. Doi and S. F. Edwards, *The Theory of Polymer Dynamics* (Clarendon Press, Oxford, 1986).
48. V. Telis, J. Telis-Romero, H. Mazzotti, and A. Gabas, Int. J. Food Prop. **10**, 185 (2007).